DALTON
FULL PAPER

Tuning solid emission by salts of the $[Pt\{4'\text{-}(o\text{-}CH_3\text{–}Ph)trpy\}Cl]^+$ and $[Pt\{4'\text{-}(o\text{-}CF_3\text{–}Ph)trpy\}Cl]^+$ luminophores: crystal structures of $[Pt\{4'\text{-}(o\text{-}CH_3\text{–}Ph)trpy\}Cl]A$ ($A = BF_4$ or SbF_6) and $[Pt\{4'\text{-}(o\text{-}CF_3\text{–}Ph)trpy\}Cl]SbF_6$ (trpy = 2,2′:6′,2″-terpyridine) †

John S. Field,[a] Raymond J. Haines,[a] David R. McMillin[b] and Grant C. Summerton[a]

[a] *School of Chemical and Physical Sciences, University of Natal, Private Bag X01, Pietermaritzburg, South Africa 3201. E-mail: field@nu.ac.za*
[b] *Department of Chemistry, Purdue University, West Lafayette, Indiana 47907-1393, USA*

Received 6th August 2001, Accepted 18th December 2001
First published as an Advance Article on the web 6th March 2002

The synthesis and characterisation of 4′-(2‴-methylphenyl)-2,2′:6′,2″-terpyridine [4′-(*o*-CH_3–Ph)trpy] and 4′-(2‴-trifluoromethylphenyl)-2,2′:6′,2″-terpyridine [4′-(*o*-CF_3–Ph)trpy] are described. Reaction of these ligands with $[Pt(PhCN)_2Cl_2]$ in the presence of the appropriate silver salt afforded $[Pt\{4'\text{-}(o\text{-}CH_3\text{–}Ph)trpy\}Cl]A$ and $[Pt\{4'\text{-}(o\text{-}CF_3\text{–}Ph)trpy\}Cl]A$ ($A = BF_4$ or SbF_6). The crystal structure of the SbF_6^- salt of the $[Pt\{4'\text{-}(o\text{-}CH_3\text{–}Ph)trpy\}Cl]^+$ cation consists of columns of cations and anions with the cations stacked parallel and head-to-tail and with a constant Pt ⋯ Pt distance [3.368(1) Å] and interplanar spacing (3.36 Å) along the stack. Crystals of the BF_4^- salt also contain columns of cations and anions with the cations stacked parallel and head-to-tail. However, the platinum atoms of successive cation pairs are offset to different extents with respect to a line drawn perpendicular to the stack. As a result the Pt ⋯ Pt distances along the stack alternate between 3.573(1) and 3.827(1) Å while the interplanar spacing is within experimental error, constant at an average value of 3.42 Å. The $[Pt\{4'\text{-}(o\text{-}CF_3\text{–}Ph)trpy\}Cl]SbF_6$ salt exhibits the same packing motif but with alternating Pt ⋯ Pt distances of 3.629(1) and 3.685(1) Å and an average interplanar spacing of 3.46 Å. The variable temperature emission spectra recorded on microcrystalline samples of these compounds reflect the environments of the cations in the crystals. The red $[Pt\{4'\text{-}(o\text{-}CH_3\text{–}Ph)trpy\}Cl]SbF_6$ salt exhibits ^{3}MMLCT (MMLCT = metal–metal–ligand-charge-transfer) emission [$\lambda(em)_{max}$ = 616 nm] that is distinguished by a large red-shift of *ca.* 60 nm in the emission maximum when the sample is cooled from room temperature to 80 K; such a red-shift is associated with strong platinum d_{z^2}–d_{z^2} orbital interactions perpendicular to the cation stack. The other three salts are yellow with broad featureless emission spectra that do not change position when the temperature is lowered but which are red-shifted when compared to the low temperature dilute glass spectrum recorded for $[Pt\{4'\text{-}(o\text{-}CH_3\text{–}Ph)trpy\}Cl]SbF_6$ in a dimethylformamide/methanol/ethanol (1 : 5 : 5) mixture; this is interpreted in terms of excimeric emission consistent with the presence of π–π interactions in the solid. The roles of the *ortho*-substituents (CH_3 and CF_3) and the anions (SbF_6^- and BF_4^-) in determining the precise arrangements of the cations in the crystals and hence the photoluminescence properties of these materials are briefly discussed.

Introduction

The solid state photoluminescence properties of mononuclear 2,2′-bipyridyl (bpy) and 2,2′:6′,2″-terpyridyl (trpy) ligand complexes of platinum(II) depend on the environment in which the luminophore finds itself in the crystalline state.[1–10] Indeed, there are few examples of compounds of this type that exhibit emission in the solid state that is not perturbed by the crystalline environment in some way, the perchlorate salt of $[Pt(bpy)(en)]^{2+}$ being a rare exception.[2] Of particular interest are compounds where the planar luminophores stack parallel to each other in the crystal with significant electronic interactions between them. Two such interactions have been identified: π–π interactions between the π-systems of adjacent ligands and platinum d_{z^2}–d_{z^2} orbital interactions along the stack.[1] The former gives rise to emission from excited state aggregates as exemplified by the solid state emission exhibited by $[Pt(phen)_2]Cl_2\cdot 3H_2O$ (phen = 1,10-phenanthroline).[2] Strong platinum d_{z^2}–d_{z^2} orbital interactions result in emission from $^3[d\sigma^*,\pi^*]$ states previously labelled as ^{3}MMLCT emission (MMLCT = metal–metal–ligand-charge transfer).[7] Both emission types typically exhibit red-shifts in their emission maxima compared to that observed when the emission is from the excited state of an isolated luminophore. A further distinguishing feature of ^{3}MMLCT emission is a red-shift in the emission maximum when the material is cooled, as evidenced by measurements over a range of temperatures of the emission spectra of the red form of $[Pt(bpy)Cl_2]$,[5,8] the orange form of $[Pt(trpy)Cl]CF_3SO_3$,[6] and the red form of $[Pt\{4'\text{-}(Ph)trpy\}]BF_4$.[10] This occurs when cooling of the crystal causes a shortening of the relevant Pt ⋯ Pt distances along the stack and a concomitant decrease in the HOMO/LUMO energy gap. Crystal structure determinations of the red form of $[Pt(bipy)Cl_2]$ at 20 and 294 K substantiate these conclusions.[8]

Of interest here are the solid state luminescence properties of the BF_4^- and SbF_6^- salts of the $[Pt\{4'\text{-}(o\text{-}CH_3\text{–}Ph)trpy\}Cl]^+$ (**1**$^+$) and $[Pt\{4'\text{-}(o\text{-}CF_3\text{–}Ph)trpy\}Cl]^+$ (**2**$^+$) cations. The platinum atoms are bound by a chloro group and by a tridentate terpyridyl ligand substituted in the 4′-position by a phenyl group itself substituted in an *ortho*-position by a bulky group, specifically by a methyl or trifluoromethyl group. *Ortho*-substitution of the 4′-phenyl ring was chosen since steric interactions between the bulky group and the 3′(5′)-proton on the central pyridine ring are expected to force the 4′-substituent to rotate around the interannular bond *i.e.*, the cationic luminophore will

† Electronic supplementary information (ESI) available: Fig. S1–3: unit cell contents of **[1]**SbF_6 viewed down the [*c*]-axis and **[1]**BF_4 and **[2]**SbF_6 viewed down the [*a*]-axis. See http://www.rsc.org/suppdata/dt/b1/b107113k/

be rendered non-planar. We wished to establish what effect this would have on the crystal structure and hence the emission, noting that the trifluoromethyl group has a larger van der Waals radius than the methyl group. A second variable is the size of the counterion, and in this work we have chosen two essentially spherical anions, one (BF_4^-) that is much smaller than the other (SbF_6^-). In order to explain the changes in the solid state emission brought about by changing these two variables, the crystal structures of [Pt{4′-(*o*-CH_3–Ph)trpy}Cl]SbF_6 ([**1**]SbF_6), [Pt{4′-(*o*-CH_3–Ph)trpy}Cl]BF_4 ([**1**]BF_4) and [Pt{4′-(*o*-CF_3–Ph)trpy}-Cl]SbF_6 ([**2**]SbF_6) have been determined.

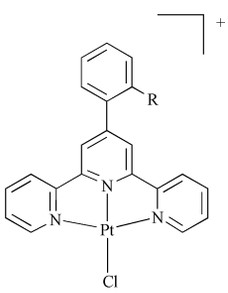

R = CH_3 (**1**$^+$) or CF_3 (**2**$^+$)

Results and discussion

The method of Kröhnke was employed for the synthesis of 4′-(2‴-methylphenyl)-2,2′:6′,2″-terpyridine [4′-(*o*-CH_3–Ph)-trpy] and 4′-(2‴-trifluoromethylphenyl)-2,2′:6′,2″-terpyridine [4′-(*o*-CF_3–Ph)trpy] and is summarised in Scheme 1.[11] Full

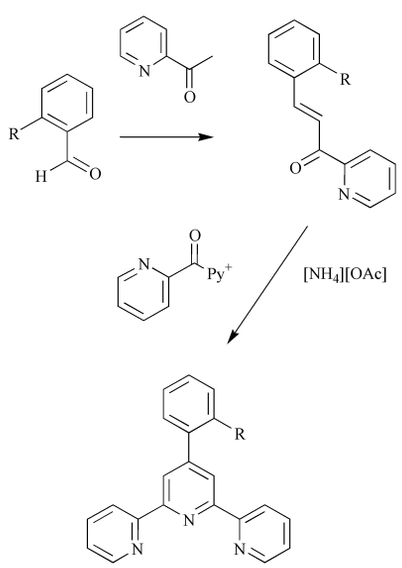

Scheme 1

details of the synthetic procedures as well as the characterisation data for both the chalcone intermediates and the ligands themselves are given in the Experimental section. Treatment of a refluxing acetonitrile solution of $[Pt(PhCN)_2Cl_2]$ with one equivalent of $AgBF_4$ or $AgSbF_6$ afforded a yellow solution and a white precipitate of silver chloride. After removal of the silver chloride one equivalent of the ligand, [4′-(*o*-CH_3–Ph)trpy] or [4′-(*o*-CF_3–Ph)trpy], was added to afford the desired product as an analytically pure, air-stable crystalline solid. Full characterisation data are given in the Experimental section. The colours of the salts are as follows: [Pt{4′-(*o*-CH_3–Ph)trpy}Cl]SbF_6 is red while [Pt{4′-(*o*-CH_3–Ph)trpy}Cl]BF_4, [Pt{4′-(*o*-CF_3–Ph)-trpy}Cl]BF_4 and [Pt{4′-(*o*-CF_3–Ph)trpy}Cl]SbF_6 are yellow.

Crystal structure of [Pt{4′-(*o*-CH_3–Ph)trpy}Cl]SbF_6 ([1]SbF_6)

Fig. 1 gives a perspective view of the cation as well as the atomic labelling scheme. A list of the important interatomic distances and angles is given in Table 1. The coordination geometry of the platinum atom is irregular square-planar, deviations from the idealised geometry being evident in the N(1)–Pt–N(2) and N(2)–Pt–N(3) angles of 81.2(3) and 80.6(4)° respectively. This is due to the geometric constraints imposed by the tridentate ligand and is typical of terpyridyl ligand complexes of platinum(II).[6,7,9,10,12] Also characteristic of a coordinated terpyridyl ligand is that the platinum to bridgehead nitrogen [N(2)] distance of 1.924(9) Å is significantly shorter than the two platinum to outer nitrogen distances of 2.019(9) [N(1)] and 2.027(11) Å [N(3)] respectively.[6,7,9,10,12] As expected the terpyridyl moiety is essentially planar with typical values for the internal bond lengths and angles.[6,7,9,10,12] However, the cation as a whole is distinctly non-planar, because the *o*-tolyl moiety is twisted about the C(8)–C(16) bond, as reflected in a dihedral angle between the mean plane through the carbon atoms of the 4′-substituent and those of the terpyridyl moiety of 65.2°. The corresponding angle measured for free 4′-phenyl-2,2′:6′,2″-terpyridine in the solid state is 10.9°,[13] and for the same ligand

Table 1 Selected interatomic distances (Å) and angles (°)

[Pt{4′-(*o*-CH_3–Ph)trpy}Cl]SbF_6, [**1**]SbF_6			
Pt–Cl	2.296(3)	Pt–N(1)	2.019(9)
Pt–N(2)	1.924(9)	Pt–N(3)	2.027(11)
C(8)–C(16)	1.50(2)		
Cl–Pt–N(1)	99.2(3)	Cl–Pt–N(2)	176.0(2)
Cl–Pt–N(3)	99.0(2)	N(1)–Pt–N(2)	81.2(3)
N(1)–Pt–N(3)	161.7(3)	N(2)–Pt–N(3)	80.6(4)
[Pt{4′-(*o*-CH_3–Ph)trpy}Cl]BF_4, [**1**]BF_4			
Pt–Cl	2.293(3)	Pt–N(1)	2.025(11)
Pt–N(2)	1.935(9)	Pt–N(3)	2.025(11)
C(8)–C(16)	1.505(14)		
Cl–Pt–N(1)	98.8(3)	Cl–Pt–N(2)	179.2(3)
Cl–Pt–N(3)	98.8(3)	N(1)–Pt–N(2)	80.6(4)
N(1)–Pt–N(3)	162.3(4)	N(2)–Pt–N(3)	81.7(4)
[Pt{4′-(*o*-CF_3–Ph)trpy}Cl]SbF_6, [**2**]SbF_6			
Pt–Cl	2.286(3)	Pt–N(1)	2.004(10)
Pt–N(2)	1.931(8)	Pt–N(3)	2.014(10)
C(8)–C(16)	1.516(14)	C(22)–F(1)	1.306(17)
C(22)–F(2)	1.337(17)	C(22)–F(3)	1.332(15)
Cl–Pt–N(1)	99.0(3)	Cl–Pt–N(2)	179.9(3)
Cl–Pt–N(3)	98.7(3)	N(1)–Pt–N(2)	81.1(4)
N(1)–Pt–N(3)	162.3(3)	N(2)–Pt–N(3)	81.2(4)

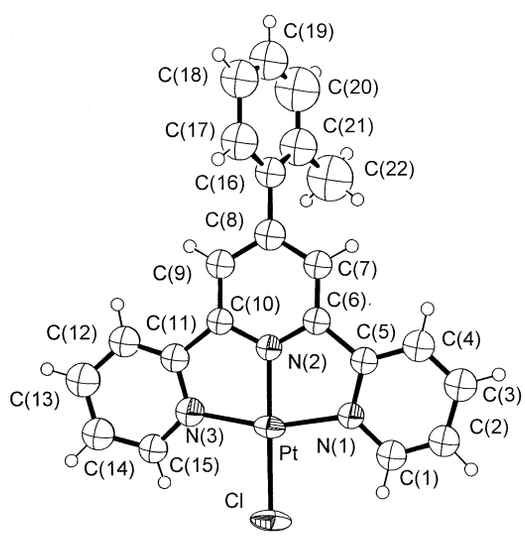

Fig. 1 ORTEP view of the cation (**1**$^+$) in [Pt{4′-(*o*-CH_3–Ph)trpy}Cl]-SbF_6. Thermal ellipsoids are drawn at the 50% probability level except for the hydrogen atoms that are shown as spheres of arbitrary radius.

coordinated to platinum in [Pt{4′-(Ph)trpy}Cl]BF_4·CH_3CN was determined as 33.4 and 33.3° for each cation in the asymmetric unit.[10] Clearly, substitution of a methyl group in the *ortho*-position of the 4′-phenyl ring causes a larger rotation about the interannular bond because of steric interactions between the methyl group and a hydrogen atom of the central pyridine ring that is also *ortho* with respect to the interannular bond. The Pt–Cl distance of 2.296(3) Å is similar to those reported for [Pt(trpy)Cl]CF_3SO_3 (2.307 Å),[6] [Pt(trpy)Cl]ClO_4 (2.302 Å)[7] and [Pt{4′-(Ph)trpy}Cl]BF_4·CH_3CN (2.296 and 2.313 Å).[10]

The crystal structure of [Pt{4′-(*o*-CH_3–Ph)trpy}Cl]SbF_6 consists of separate columns of cations and anions stacked parallel to the [*c*]-axis of the unit cell (Fig. S1†). The cations stack in such a way that the mean planes through the platinum, chlorine and terpyridyl moiety atoms (*i.e.*, excluding the atoms of the 4′-group) are parallel to each other and perpendicular to the [*c*]-axis. Fig. 2 illustrates one cation pair viewed perpendicular to the stack. As required by the presence of a two-fold screw axis along [*c*] the platinum atoms along the stack are equally spaced, an arrangement that is usually described as a *linear chain structure*.[1,8] The Pt ··· Pt distance is 3.368(1) Å while the Pt ··· Pt ··· Pt angle of 162° indicates that successive platinum atoms are almost eclipsed when viewed down the stacking axis (Fig. 2). Given that the Pt ··· Pt distance is similar to values normally taken to indicate a strong σ-interaction between overlapping platinum d_{z^2}-orbitals,[1,14] this implies direct and strong overlap of the platinum d_z^2-orbitals along the stack. As described below this has a dramatic effect on the emission properties of the solid. The perpendicular distance between the mean planes through the platinum, chlorine and terpyridyl moiety atoms of adjacent cations (the interplanar spacing) is 3.33 Å (= *c*/2). This is considerably less than the value of *ca.* 3.8 Å usually taken as the upper distance limit for π–π interactions in organic species,[15] and could be taken to imply that π–π interactions are important in determining the photophysical properties of the salt. However, as noted below, it is the strong platinum d_{z^2}–d_{z^2} orbital interactions that are largely responsible for the photoluminescence behaviour of this salt.

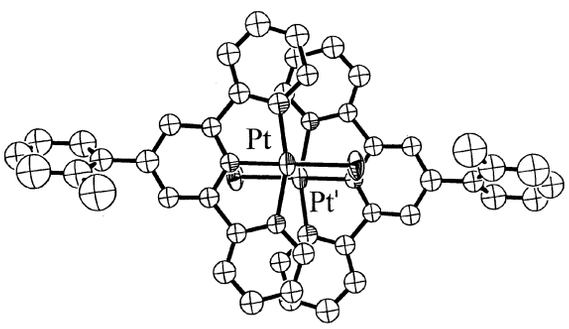

Fig. 2 ORTEP diagram showing a cation–cation interaction in [Pt{4′-(*o*-CH_3–Ph)trpy}Cl]SbF_6 perpendicular to the mean planes through the platinum, chlorine and terpyridyl moiety atoms.

The structure of [Pt{4′-(*o*-CH_3–Ph)trpy}Cl]SbF_6 is unusual in that terpyridyl ligand complexes of platinum(II) either do not exhibit stacked structures or if a stacked structure is observed the Pt ··· Pt distances are not uniformly equal along the stacking direction. This contrasts the situation for α-diimine complexes of platinum(II) for which there are several well-documented examples with linear chain structures.[16] Other examples of terpyridyl ligand complexes of platinum(II) with stacked structures are the triflate and perchlorate salts of the [Pt(trpy)Cl]$^+$ cation;[6,7] both consist of discrete Pt_2 units arranged along an infinite trpy-π stack. Uniform spacing of the platinum atoms is also not observed for the low temperature crystal structure of [Pt{4′-(Ph)trpy}Cl]BF_4·CH_3CN where the stacking motif comprises a series of tetramers with an internal Pt ··· Pt separation of 3.33 Å and an inter-tetramer separation of 3.62 Å.[10]

Crystal structure of [Pt{4′-(*o*-CH_3–Ph)trpy}Cl]BF_4 ([1]BF_4)

The cation atomic labelling scheme is the same as that illustrated in Fig. 1. A list of the important interatomic distances and angles is given in Table 1. There are no significant differences between these values and those listed in Table 1 for the SbF_6^- salt and the same comments therefore apply to both sets of geometric parameters (*vide supra*). However, one intramolecular parameter that is particularly sensitive to packing effects and so possibly influenced by a change in the size of the anion, is the dihedral angle between the mean plane through the non-hydrogen atoms of the 4′-substituent and the mean plane through the non-hydrogen atoms of the terpyridyl moiety. This angle is 69.9° *i.e.*, about 5° larger than the corresponding angle of 65.2° measured for the SbF_6^- salt.

The BF_4^- salt also has the cations stacked parallel and head-to-tail with the anions occupying channels between the cation stacks (Fig. S2†). However, there are important differences of detail compared to those observed for the SbF_6^- salt. First, the mean plane through the platinum, chlorine and terpyridyl moiety atoms is within experimental error perpendicular to the [*a*]-axis with successive cations related by a centre of inversion rather than a two-fold screw axis. Second, the Pt ··· Pt distances along the stack are not uniformly equal but alternate between values of 3.573(1) and 3.827(1) Å. On the other hand, the mean planes are within experimental error equally spaced, with an averaged interplanar spacing of 3.42 Å. The packing motif of [Pt{4′-(*o*-CH_3–Ph)trpy}Cl]BF_4 is therefore very similar to that reported for the triflate and perchlorate salts of the [Pt(trpy)Cl]$^+$ cation.[6,7] Fig. 3 gives views perpendicular to the mean planes through the platinum, chlorine and non-hydrogen atoms of the terpyridyl moiety for each of the two different cation–cation interactions along the stack. The extent of slippage of adjacent cations with respect to a line perpendicular to the stack determines the Pt ··· Pt distance for a pair of cations. The shorter distance of 3.573(1) Å is too long to support effective overlap between the platinum d_{z^2}-orbitals,[14] especially as the orbitals are not lined-up in the same direction because of the lateral offset of adjacent cations. Clearly the same is true for the pair of cations with the longer Pt ··· Pt distance of 3.827(1) Å. In so far as π–π interactions along the stack are concerned the following comments apply. The interplanar spacing of 3.42 Å is short enough to support π–π interactions being well within the upper distance limit of 3.8 Å for π-interactions between organic species.[15] However, in the absence of detailed calculations on the nature of the π-interactions in stacked terpyridines, we are uncertain of the optimum geometry for a favourable π-interaction. What is certain is that even large lateral offsets in stacked porphyrins allow for a relatively strong electrostatic attraction between the π-systems of adjacent ligands.[15] Also, the emission data obtained on microcrystalline samples (*vide infra*) suggest that intermolecular π–π interactions are important in determining the photoluminescence behaviour of [Pt{4′-(*o*-CH_3–Ph)trpy}Cl]BF_4.

The question arises as to why, by replacing the larger SbF_6^- with the smaller BF_4^- anion while retaining the same [Pt{4′-(*o*-CH_3–Ph)trpy}Cl]$^+$ cation, the crystal structure changes from a linear chain with a uniform Pt ··· Pt distance along the stack to one where the Pt ··· Pt distances alternate along an infinite π-stack? We first note that the structural change is brought about by the parallel planes of cations slipping past each other in such a way that for successive pairs of cations the extent of slippage is not the same. Also significant is that slippage of this kind removes the possibility of extended platinum d_{z^2}–d_{z^2} orbital interactions along the stack; yet these interactions are regarded as the most important in so far as stabilising a linear chain structure is concerned.[16] Other factors that are expected

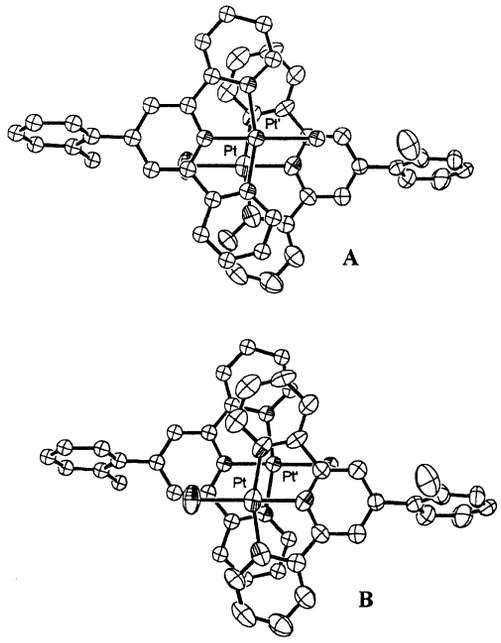

Fig. 3 ORTEP diagrams showing the two types of cation–cation interactions along the [Pt{4′-(*o*-CH_3–Ph)trpy}Cl]$^+$ stacks in [Pt{4′-(*o*-CH_3–Ph)trpy}Cl]BF_4 viewed perpendicular to the mean planes through the platinum, chlorine and non-hydrogen atoms of the terpyridyl moiety: A, Pt ··· Pt distance = 3.573 ; B, Pt ··· Pt distance = 3.827. The perpendicular distances between the mean planes are nearly identical for interaction A (3.40) and interaction B (3.44). Atoms are shown as 40% probability ellipsoids. Hydrogen atoms are omitted.

to play a role in determining the dimensions of the stack are steric repulsions and intermolecular forces, both attractive and repulsive.[16] The former should not be responsible for initiating the structural change given that the cation remains the same, in particular with regard to the methyl substituent in the *ortho*-position of the 4′-phenyl ring. As far as intermolecular forces are concerned it is possible that a strengthening of attractive intermolecular forces of the π–π type helps drive the structural change but, without detailed lattice energy calculations, this must be regarded as a tentative conclusion. What is clear however, is that the structural change brings about an improvement in the packing efficiency. This is evident from a comparison of the densities of the two solids: for the SbF_6^- salt it is 2.21 g cm^{-3} while for the BF_4^- salt it is 1.97 g cm^{-3}. Were BF_4^- anions to replace the SbF_6^- anions in the crystal structure of the SbF_6^- salt the density would be only 1.79 g cm^{-3}.

Crystal structure of [Pt{4′-(*o*-CF_3–Ph)trpy}Cl]SbF_6 ([2]SbF_6)

Fig. 4 gives a perspective view of the cation as well as of the atomic numbering scheme. A list of selected interatomic distances and angles is given in Table 1. The coordination geometry of the platinum atom and the bond lengths and angles internal to the substituted terpyridyl ligand are typical of those discussed above for [Pt{4′-(*o*-CH_3–Ph)trpy}Cl]SbF_6 and for terpyridyl ligand complexes of platinum(II) in general.[6,7,9,10,12] Of particular interest is the dihedral angle between the mean planes through the carbon atoms of the 4′-substituent on one hand and those of the terpyridyl moiety on the other. This is 62.1°, a smaller value than those of 65.2 and 69.9° obtained for the SbF_6^- and BF_4^- salts of the [Pt{4′-(*o*-CH_3–Ph)trpy}Cl]$^+$ cation respectively, an unexpected result given that the van der Waals radius of a trifluoromethyl group is larger than that of a methyl group and that steric repulsions involving the 3′(5′)-hydrogen of the central pyridine ring will therefore be greater with the trifluoromethyl group than with the methyl group. Presumably, the unexpectedly smaller angle is a consequence of packing effects as discussed below.

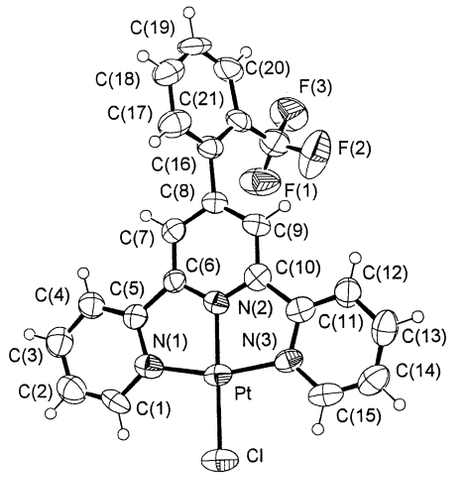

Fig. 4 ORTEP view of the cation (**2**$^+$) in [Pt{4′-(*o*-CF_3–Ph)trpy}Cl]-SbF_6. Thermal ellipsoids are drawn at the 50% probability level except for the hydrogen atoms that are shown as spheres of arbitrary radius.

The overall packing motif exhibited by the cations and anions in [Pt{4′-(*o*-CF_3–Ph)trpy}Cl]SbF_6 is very similar to that for [Pt{4′-(*o*-CH_3–Ph)trpy}Cl]BF_4, the only differences being in the precise dimensions for the cation stack. Thus the cations stack parallel and head-to-tail with the anions occupying channels between the cation stacks (Fig. S3 †); the mean planes through the platinum, chlorine and terpyridyl moiety atoms are perpendicular to the [*a*]-axis and are within experimental error equally spaced; and the Pt ··· Pt distances alternate along the stack. The Pt ··· Pt distances are 3.629(1) and 3.685(1) Å and the interplanar spacings averages at 3.46 Å. Noteworthy is that the Pt ··· Pt distances are more nearly equal than those determined for the tetrafluoroborate salt. Fig. 5 illustrates the two different cation–cation interactions along the stack taking a view perpendicular to the mean planes through the platinum,

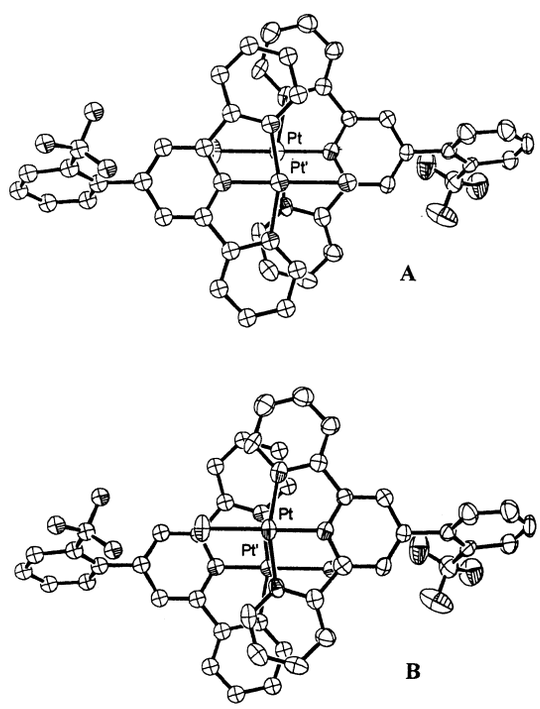

Fig. 5 ORTEP diagrams showing the two types of cation–cation interactions along the [Pt{4′-(*o*-CF_3–Ph)trpy}Cl]$^+$ stacks in [Pt{4′-(*o*-CF_3–Ph)trpy}Cl]SbF_6 viewed perpendicular to the mean plane through the platinum, chlorine and non-hydrogen atoms of the terpyridyl moiety: A, Pt ··· Pt distance = 3.629; B, Pt ··· Pt distance = 3.685 . The perpendicular distances between the mean planes are nearly identical for interaction A (3.45) and interaction B (3.47). Atoms are shown as 40% probability ellipsoids. Hydrogen atoms are omitted.

chlorine and non-hydrogen atoms of the terpyridyl moiety. The lateral offset of the platinum atoms and the long Pt ··· Pt distances preclude any significant overlap of platinum d_{z^2}-orbitals perpendicular to the stack. The interplanar spacing falls within the upper distance limit of 3.8 Å for π-interactions between organic species.[15] Following the same line of reasoning given above for [Pt{4′-(*o*-CH_3–Ph)trpy}Cl]BF_4 we tentatively conclude that π–π interactions play a role in determining the crystal structure and photophysical properties of the salt (*vide infra*).

The question arises as to why, by replacing a methyl with a trifluoromethyl group as the *ortho*-substituent on the 4′-ring while retaining the same SbF_6^- anion, the crystal structure changes from linear chain with a uniform Pt ··· Pt distance along the stack to one where the Pt ··· Pt distances alternate along an infinite π-stack? Again the structural change is brought about by the parallel planes of cations slipping past each other in such a way that for successive pairs of cations the extent of slippage is not the same; at the same time, extended platinum d_{z^2}–d_{z^2} orbital interactions along the stack are lost. Steric factors are probably important here as the methyl group with a van der Waals radius of 2.0 Å is somewhat smaller than a trifluoromethyl group with a van der Waals radius of 2.3 Å.[17] Evidence for this comes from consideration of the non-bonded contact distance between the carbon atom of the trifluoromethyl group [C(22)] and the chlorine atom of the cation in the next layer (Fig. 5). This distance is 4.27 Å, a value that is close to the sum of the van der Waals radii for a trifluoromethyl group and a chlorine atom of 4.2 Å.[17,18] It would appear that the C(22) ··· Cl′ contact prevents the cations from sliding into a position that allows for directed platinum d_{z^2}-orbital interactions perpendicular to the stack. Interestingly, the C(22) ··· Cl′ distance is linked to the angle of rotation of the 4′-group about the interannular bond; the smaller the angle the larger the distance. As noted above, the dihedral angle of 62.1° observed for [**2**]SbF_6 is smaller than those of 65.2 and 69.9° observed for [**1**]SbF_6 and [**1**]BF_4 respectively, despite the fact that the trifluoromethyl group is sterically more demanding than the methyl group.

Photophysical properties

The absorption spectra measured in acetonitrile are nearly identical for all four of the salts and, moreover, are very similar to those recorded in acetonitrile for salts of the $[Pt(trpy)Cl]^+$ [6,7] and $[Pt(4'\text{-Ph–trpy})Cl]^+$ [6,10] luminophores. Accordingly, the same assignments are made. The relatively sharp band at *ca.* 280 nm and the vibrationally structured band with maxima in the range 300–350 nm are attributed to $^1(\pi–\pi)$ transitions of the substituted terpyridyl ligands, while the two less intense and poorly resolved peaks at wavelengths greater than 350 nm are assigned to Pt(5d)⟶trpy(π*) (^{1}MLCT) transitions. Data are given in the Experimental section. None of the salts gives rise to detectable emission when dissolved in degassed acetonitrile and irradiated with light of 330 nm wavelength at room temperature. Salts of the $[Pt(trpy)Cl]^+$ [6,7] and $[Pt(4'\text{-Ph–trpy})Cl]^+$ [6,10] luminophores also do not display emissions in degassed acetonitrile at room temperature; on the other hand salts of the [Pt{4′-(*p*-R–Ph)trpy}Cl]$^+$ (R = CH_3, OCH_3, Br, or CN) luminophores do give rise to emission in degassed acetonitrile.[6] When fluid emission by monomers of platinum(II) is not observed one explanation is that low-lying d–d excited states provide facile and non-radiative deactivation pathways *via* molecular distortions,[19a] while another is that axial interactions involving the donor solvent quench emissions by the excited state monomer.[19b] Unfortunately, because of solubility problems, it was not possible to measure emission spectra in a non-coordinating solvent such as dichloromethane and we are therefore uncertain as to the reason for the lack of fluid emission by salts of the [Pt{4′-(*o*-R–Ph)trpy}Cl]$^+$ (R = CH_3 or CF_3) chromophores.

The emission spectra measured over a range of temperatures on a microcrystalline sample of the red [Pt{4′-(*o*-CH_3–Ph)-trpy}Cl]SbF_6 salt are shown in Fig. 6. Also shown in Fig. 6 is

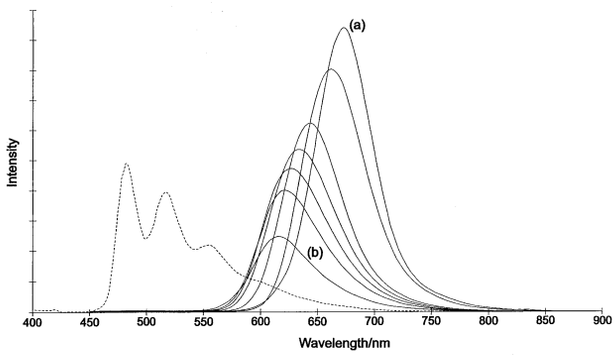

Fig. 6 Dilute (0.01 mM) dimethylformamide/methanol/ethanol (1 : 5 : 5) glass emission spectrum recorded at 77 K (···) and solid state emission spectra recorded at 40 K intervals over the range 80 (a) to 280 K (b) (—) of [Pt{4′-(*o*-CH_3–Ph)trpy}Cl]SbF_6. λ_{ex} = 330 nm.

the emission spectrum of the same salt recorded in a dilute (0.01 mM) dimethylformamide/methanol/ethanol (1 : 5 : 5) glass at 77 K. The dilute glass spectrum reflects emission by the [Pt{4′-(*o*-CH_3–Ph)trpy}Cl]$^+$ luminophores when they are in a monomeric environment,[19c] and thus comparison of the glass spectrum with that recorded in the solid state can provide information on the effect of solid state interactions on the electronic structure of the luminophore.[2] The vibrationally structured glass spectrum is very similar to that recorded for [Pt(trpy)Cl]CF_3SO_3 in a dilute butyronitrile glass at 77 K.[3] On this basis we make the same assignment which is that the glass emission for [**1**]SbF_6 derives from an essentially intraligand $^3(\pi–\pi^*)$ excited state.[6] Turning to the emission recorded for the solid (Fig. 6) we first note that there is a substantial red-shift compared to that observed for the glass, an observation that suggests that solid state interactions are important in determining the emission properties of the salt. The 280 K spectrum consists of a broad asymmetric peak centred at 616 nm that is devoid of any vibrational structure. On cooling the sample to 80 K the peak increases in intensity, narrows and shifts dramatically to the red, specifically from a peak maximum of 616 nm at 280 K to 673 nm at 80 K. These data and, in particular the red-shift observed on cooling, are strongly suggestive of emission from a $^3[d\sigma^*,\pi^*]$ (^{3}MMLCT) state. Also consistent with emission from a $^3[d\sigma^*,\pi^*]$ state is the narrowing of the band on cooling.[1,9,10] Furthermore, the solid state structure of the compound shows a Pt ··· Pt distance along a uniform stack of luminophores that is short enough [3.368(1) Å] to support strong platinum d_{z^2}–d_{z^2} orbital interactions along the stack; a requirement for ^{3}MMLCT emission. Similar solid state luminescence behaviour by the orange triflate salt of the $[Pt(trpy)Cl]^+$ luminophore,[6] as well as by the red form of [Pt(bipy)Cl_2][8] has also been attributed to emissions from ^{3}MMLCT states. Noteworthy, is the systematic increase in intensity of the emission on lowering the temperature. Linked to this trend is a ten-fold increase in the emission lifetime from 155 ns at 295 K to 1680 ns at 77 K. The solid state emission data recorded for [Pt{4′-(*o*-CH_3–Ph)trpy}Cl]SbF_6 as well as for the other salts studied in this work are summarised in Table 2.

The variable temperature emission spectra measured on a microcrystalline sample of the yellow [Pt{4′-(*o*-CH_3–Ph)trpy}-Cl]BF_4 salt are shown in Fig. 7. The 280 K spectrum consists of a relatively broad (full-width-at-half-maximum = 2508 cm^{-1}) asymmetric band that is devoid of vibrational structure. On lowering the temperature of the sample there is a systematic increase in the intensity, slight narrowing of the band but no red-shift in the emission maximum. In assigning the origin of the emission we note that there is a substantial red-shift in

Table 2 Emission data[a]

	$\lambda(em)_{max}$/nm[b]	fwhm/cm^{-1}[b,c]	τ/ns[d]
[**1**](SbF_6)	616[673]	1635[1119]	155[1680]
[**1**](BF_4)	564[566]	2508[2109]	348[2880]
[**2**](SbF_6)	589[589]	2735[2596]	325[2620]
[**2**](BF_4)	571[571]	3100[2450]	not measured

[a] Measured on microcrystalline samples. [b] At 280 K. Data recorded at 80 K are given in square brackets. [c] fwhm = full-width-at-half-maximum. [d] At 295 K. Data recorded at 77 K are given in square brackets.

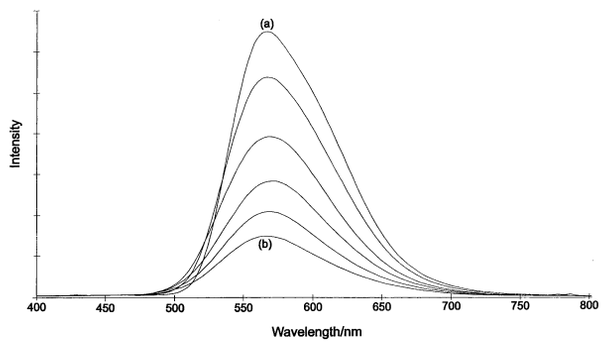

Fig. 7 Solid state emission spectra of [Pt{4′-(*o*-CH_3–Ph)trpy}Cl]BF_4 recorded at 40 K intervals over the range 80 (ka) to 280 K (b). λ_{ex} = 330 nm.

the band position compared to that recorded for the [Pt{4′-(*o*-CH_3–Ph)trpy}Cl]$^+$ cation in a dilute glass (Fig. 6); also that the vibrational structure present in the glass spectrum and characteristic of monomeric intraligand π–π* emission is no longer present. These observations lead to the conclusion that solid state interactions are important in determining the emission properties of the solid and that monomer emission in the solid is unlikely. In view of the long Pt ··· Pt distances in the crystal (*vide supra*) platinum d_{z^2}–d_{z^2} orbital interactions can be ruled out. Moreover the emission behaviour, especially with regard to the lack of any dependence of the wavelength of the emission maximum on temperature, bears no resemblance to that expected for ^{3}MMLCT emission. On the other hand there is evidence from the crystal structure analysis for extended π–π interactions in the solid (*vide supra*). On this basis emission from a π-dimer that forms when the compound is irradiated must be considered as a possibility.[1,2] Indeed, the presence of closely stacked layers of cations in [**1**]BF_4 appears to mandate the formation of excited state dimers (excimers) but almost certainly not with the geometry that is ideal for the excited state. The inevitable mismatch between the ground and excited state potential energy surfaces will in turn promote structural relaxation in the excited state and loss of vibrational structure in the emission spectrum. This explains the broad featureless appearance of the emission band that is generally regarded as typical of excimer emission; for example, excimer emission by [Pt(phen)$_2$]Cl_2·$3H_2O$[2] as well as by the orange Cl^-, ClO_4^-, $CF_3SO_3^-$ and yellow PF_6^- salts of the [Pt(trpy)Cl]$^+$ cation[7] is also broad and featureless. Also typical of excimer emission is a red-shift in the emission maximum compared to that observed for the isolated chromophore.[1,2] Taken together the evidence suggests that the solid state emission exhibited by [**1**]BF_4 is largely excimeric in origin.[19d]

Both the SbF_6^- and BF_4^- salts of the [Pt{4′-(*o*-CF_3–Ph)-trpy}Cl]$^+$ luminophore are yellow and, moreover, both exhibit luminescence behaviour in the solid state very similar to that measured for [Pt{4′-(*o*-CH_3–Ph)trpy}Cl]BF_4; the emission data are summarised in Table 2. The emission bands are asymmetric, unstructured, relatively broad and red-shifted with respect to the dilute glass emission shown in Fig. 6; cooling the compounds to 80 K has no effect on the position of the emission band. Applying the same arguments used to interpret the emission spectra measured for [Pt{4′-(*o*-CH_3–Ph)trpy}Cl]BF_4 leads to the conclusion that [Pt{4′-(*o*-CF_3–Ph)trpy}Cl]SbF_6 and [Pt{4′-(*o*-CF_3–Ph)trpy}Cl]BF_4 also exhibit solid emission that is largely excimeric in origin. Support for this conclusion comes from the results of the crystal structure determination of [Pt{4′-(*o*-CF_3–Ph)trpy}Cl]SbF_6 that suggest the existence of intermolecular trpy π–π interactions in the solid state (*vide supra*).

Concluding remarks

The crystal structures of [**1**]SbF_6, [**1**]BF_4 and [**2**]SbF_6 all consist of separate and parallel columns of cations and anions. Also common to all three structures is that the cations stack parallel to each other in the head-to-tail orientation that allows the out-of-plane 4′-group to point towards a "hole" in the adjacent cation layer; indeed, the head-to-tail arrangement appears to be a necessary consequence of the out-of-plane twisting of the 4′-group. These structural features are in accord with the principle that free volume in crystals is energetically unfavourable.[20] Two variables have been used to alter the geometry of a cation stack. The first is the choice of anion. Changing the anion from SbF_6^- to BF_4^- while retaining the same cation disrupts the uniform stacking of the platinum atoms, as evidenced by different lateral offsets of the platinum atoms in successive pairs of cations with respect to a line perpendicular to the stacking planes. The second is the choice of R-group in the *ortho*-position of the 4′-phenyl ring. Changing a methyl group for a trifluoromethyl group while retaining the same SbF_6^- anion, disrupts the uniform stacking of the platinum atoms in the same way but for different reasons. We have also learnt from this work that the choice of the fourth ligand bonded to platinum, in particular its size and/or ability to bond to the R-group, will play a role in determining the precise dimensions of the stack. Thus, by suitable choice of R-group, anion and the fourth ligand bonded to platinum it is possible to fine-tune the dimensions of the cation stack and hence the photoluminescence properties of the salt. Of particular interest are the structural requirements for ^{3}MMLCT emission by stacked terpyridyl ligand complexes of platinum(II). This work as well as that by others,[4–8,16] confirms that the stack must include a Pt ··· Pt distance that is short enough to support d_{z^2}–d_{z^2} orbital interactions perpendicular to the stack, the upper distance limit being about 3.5 Å. A second structural requirement is that the closely-spaced platinum atoms must be positioned such that their d_{z^2}-orbitals point towards each other. Note that these two requirements do not place restrictions on the pattern of Pt ··· Pt distances along the stack. For example, a linear chain structure where the Pt ··· Pt distances are all the same is not a pre-condition for ^{3}MMLCT emission; nor is it a pre-condition for a red-shift in the emission maximum when the material is cooled as evidenced by the temperature dependence of the ^{3}MMLCT emission exhibited by [Pt(trpy)Cl]CF_3SO_3[6] and [Pt(4′-Ph-trpy)Cl]BF_4·CH_3CN[10] neither of which has a linear chain structure. We finally note that in terms of the Peierls theorem one dimensional structures with equal separations of the repeating units are not intrinsically stable;[21] as the temperature of the material is lowered distortions are anticipated that will lead to the formation of molecular units along the stack. Based on the limited structural data available so far for terpyridyl ligand complexes of platinum(II) these may be Pt_2 dimers[6,7] or Pt_4 tetramers.[10]

Experimental

Materials

Reagents for the ligand syntheses were obtained and used as follows: The 2-acetylpyridine was obtained commercially

(Fluka) and used without further purification; the 2-tolualdehyde (Merck) and α,α,α-trifluoro-2-tolualdehyde (Aldrich) were also obtained commercially both being further purified by distillation; the *N*-{1-(2′-pyridyl)-1-oxo-2-ethyl}pyridinium iodide was synthesised by the method of Kröhnke.[11] All manipulations for the complex salt syntheses were performed under an atmosphere of nitrogen using standard Schlenk tube techniques. The acetonitrile used as the solvent and for the purposes of crystal growth was purified by the method of Carlsen *et al.*[22] The dichlorobis(benzonitrile)platinum(II) (Strem) and the silver salts $AgSbF_6$ and $AgBF_4$ (Fluka) were used without further purification.

Physical measurements and instrumentation

Microanalyses for %C, H and N were performed by the microanalytical laboratory at the University of Natal, Pietermaritzburg and by Galbraith Laboratories Inc., Knoxville, Tennessee, USA. Melting points were recorded on a Kofler hot stage apparatus and are uncorrected. ^{1}H NMR (200 MHz) spectra were recorded on a Varian Gemini 200 spectrometer at 25 °C with chemical shifts referenced to $SiMe_4$. Infrared spectra were recorded as KBr discs on a Shimadzu FTIR-4300 spectrometer. Mass spectra were obtained on a Hewlett Packard GCMS using electron impact (EI) ionisation. UV/vis absorption spectra were recorded at 22 °C using a Shimadzu UV-2101PC scanning spectrophotometer. Emission spectra were recorded on a SLM-Amico SPF 500C fluorometer at 22 °C unless otherwise stated. Deoxygenated spectroscopic grade solvents were used for both the absorption and emission measurements. Solid state emission spectra were recorded on microcrystalline samples. For the variable temperature emission measurements the cryostat was an Oxford Instruments DN1704 liquid-nitrogen-cooled system complete with an Oxford Instruments temperature controller. The excitation wavelength was 330 nm, with the scattered light removed by a 400 nm long-wave-pass filter. The 337 nm line from a nitrogen laser served as the excitation source for the lifetime measurements, with a 337 nm band pass filter used to remove stray light from the beam. Lifetime data were analysed as described previously.[23]

Syntheses

2-R-1-{3-(2-pyridyl)-3-oxopropenyl}benzene (R = CH_3 or CF_3). A solution of 2-R-benzaldehyde (20 mmol) in absolute ethanol (100 mL) was cooled to 0 °C and 2-acetylpyridine (2.42 g, 20 mmol) added. Aqueous sodium hydroxide (20 mL, 1.0 M) was then added dropwise and the reaction mixture stirred at 0 °C for 3 h. This resulted in the separation of a light yellow precipitate that was collected by filtration, washed with ethanol and dried *in vacuo*. Yields: R = CH_3 (4.30 g, 96%); R = CF_3 (5.39 g, 97%). Mp's: R = CH_3 (68 °C); R = CF_3 (63 °C). Anal. R = CH_3 (Calcd. for $C_{15}H_{13}NO$: C 80.7; H 5.9; N 6.3. Found: C 80.8; H 5.8; N 6.2%). R = CF_3 (Calcd. for $C_{15}H_{10}F_3NO$: C 65.0; H 3.6; N 5.1. Found: C 64.8; H 3.6; N 5.1%). MS(EI) *m*/*z*: R = CH_3 (223, M^+); R = CF_3 (277, M^+). IR (KBr, cm^{-1}): R = CH_3 [*ν*(CO) 1670s]; R = CF_3 [*ν*(CO) 1680s].

4′-(C_6H_4R-*o*)-2,2′:6′,2″-terpyridine (R = CH_3 or CF_3). *N*-{1-(2′-pyridyl)-1-oxo-2-ethyl}pyridinium iodide (0.68 g, 2.2 mmol) and ammonium acetate (10 g, excess) were added to a suspension of 2-R-{3-(2-pyridyl)-3-oxopropenyl}benzene (2.0 mmol) in absolute ethanol (8 mL) and the mixture heated at reflux for 40 min. An off-white solid precipitated on cooling. This was collected by filtration, washed with 50% aqueous ethanol and dried *in vacuo*. Recrystallisation from ethanol afforded colourless crystals of the desired ligands. Yields: R = CH_3 (0.31 g, 47%); R = CF_3 (0.41 g, 54%). Mp's: R = CH_3 (156 °C); R = CF_3 (148 °C). Anal. R = CH_3 (Calcd. for $C_{22}H_{17}N_3$: C 81.7; H 5.3; N 13.0. Found: C 81.6; H 5.0; N 13.0%). R = CF_3 (Calcd. for $C_{22}H_{14}F_3N_3$: C 70.0; H 3.7; N 11.1. Found: C 69.9; H 3.9; N 11.0%). MS(EI) *m*/*z*: R = CH_3 (323 M^+); R = CF_3 (377, M^+). ^{1}H NMR ($CDCl_3$): R = CH_3 [*δ* 8.71 (m, 2 H, $H_{6,6''}$); 8.67 (m, 2 H, $H_{3,3''}$); 8.47 (s, 2 H, $H_{3',5'}$); 7.87 (m, 2 H, $H_{4',4''}$); 7.32 (m, 4 H, C_6H_4); 7.30 (m, 2 H, $H_{5,5''}$); 2.37 (s, 3 H, CH_3)]. R = CF_3 [*δ* 8.72 (m, 2 H, $H_{6,6''}$); 8.70 (m, 2 H, $H_{3,3''}$); 8.54 (s, 2 H, $H_{3',5'}$); 7.84 (m, 2 H, $H_{4,4''}$); 7.54 (m, 4 H, C_6H_4); 7.35 (m, 2 H, $H_{5,5''}$)]. UV/vis (CH_3CN): λ_{max}/nm (ε/M^{-1} cm^{-1}): R = CH_3 [303(sh, 1.6×10^4); 277(3.0×10^4); 250(3.5×10^4)]. R = CF_3 [303(sh, 1.3×10^4); 277(2.9×10^4); 239 (3.4×10^4); 208 (3.6×10^4)].

[Pt{4′-(*o*-R–Ph)trpy}Cl]A (R = CH_3 or CF_3; A = SbF_6 or BF_4). A suspension of $[Pt(PhCN)_2Cl_2]$ (0.10 g, 0.21 mmol) in acetonitrile (10 mL) was treated with an equimolar amount of AgA (0.073 g for A = SbF_6; 0.041 g for A = BF_4) dissolved in acetonitrile (5 mL). The reaction mixture was heated under reflux for 16 h, the AgCl precipitate removed by filtration and one equivalent of 4′-(C_6H_4R-*o*)-2,2′:6′,2″-terpyridine (0.060 g for R = CH_3; 0.080 g for R = CF_3) added to the filtrate. The reaction mixture was heated under reflux for an additional 24 h after which the volume was reduced *in vacuo*, the solution cooled to room temperature and allowed to stand for a further 24 h. This resulted in the precipitation of [Pt{4′-(*o*-R–Ph)-trpy}Cl]A. The precipitate was washed with cold acetonitrile (*ca.* 5 mL) and diethyl ether (*ca.* 10 mL) and dried *in vacuo* to afford an analytically pure microcrystalline product. Yields and colours: R = CH_3, A = SbF_6 (0.14 g, 84%, red); R = CH_3, A = BF_4 (0.10 g, 78%, yellow); R = CF_3, A = SbF_6 (0.14 g, 76%, yellow); R = CF_3, A = BF_4 (0.13 g, 89%, yellow). Anal. R = CH_3, A = SbF_6 (Calcd. for $C_{22}H_{17}ClF_6N_3PtSb$: C 33.4; H 2.3; N 5.3. Found: C 33.1; H 1.9; N 5.2%). R = CH_3, A = BF_4 (Calcd. for $C_{22}H_{17}BClF_4N_3Pt$: C 41.8; H 2.9; N 6.7. Found: C 41.6; H 2.9; N 6.6%). R = CF_3, A = SbF_6 (Calcd. for $C_{22}H_{14}ClF_9N_3PtSb$: C 31.3; H 1.8; N 5.0. Found: C 31.3; H 1.4; N 4.9%). R = CF_3, A = BF_4 (Calcd. for $C_{22}H_{14}BClF_7N_3Pt$: C 38.0; H 2.2; N 6.0. Found: C 38.0; H 2.0; N 5.9%). ^{1}H NMR ($CDCl_3$): R = CH_3, A = SbF_6 [*δ* 2.43 (s, 3 H, CH_3); 7.45 (m, 4 H, aromatic C*H*); 7.74 (m, 2 H, aromatic C*H*); 8.25 (m, 6 H, aromatic C*H*); 8.84 (m, 2 H, aromatic C*H*)]. R = CF_3, A = SbF_6 [*δ* 7.6–8.2 (m, 6 H, aromatic C*H*); 8.45 (m, 2 H, aromatic C*H*); 8.64 (m, 2 H, aromatic C*H*); 8.79 (m, 4 H, aromatic C*H*)]. IR (KBr, cm^{-1}): R = CH_3, A = SbF_6 [*ν*{4′-(*o*-CH_3–Ph)trpy} 1618s, 1557m, 1477m, 1419m, 1035m, 888m; *ν*(SbF_6^-) 659vs]. R = CH_3, A = BF_4 [*ν*(BF_4^-) 1064vs]. R = CF_3, A = SbF_6 [*ν*{4′-(*o*-CF_3–Ph)trpy} 1611s, 1478m, 1422m, 1319m, 1179m; *ν*(SbF_6^-) 661vs]. R = CF_3, A = BF_4 [*ν*(BF_4^-) 1061vs]. UV/vis (CH_3CN): λ_{max}/nm (ε/M^{-1} cm^{-1}): R = CH_3, A = SbF_6 [283(3.1×10^4); 307(1.7×10^4); 316(1.7×10^4); 332(1.9×10^4); 347(7.6×10^3); 380(4.2×10^3); 399(4.5×10^3)]. R = CF_3, A = SbF_6 [285(3.8×10^4); 306(1.3×10^4); 319(1.2×10^4); 332(1.6×10^4); 349(7.6×10^3); 381(3.4×10^3); 396(3.4×10^3)].

Crystal structure determinations

Needle-shaped crystals of [**1**]SbF_6 (red), [**1**]BF_4 (yellow) and [**2**]SbF_6 (yellow) were grown by slow evaporation at room temperature of a saturated solution of the compound in acetonitrile. Crystal data and details of the crystallographic studies are reported in Table 3. Intensity data were obtained on an Enraf-Nonius CAD4 diffractometer, using graphite monochromated MoKα radiation and the *ω*–2*θ* scan technique. Unit cell parameters were obtained by least squares fitting of 25 reflections monitored in the range $3° < \theta < 12°$ while the diffraction data were collected in the range $2° < \theta < 23°$. Corrections for Lorentz, polarisation, and absorption (*χ* scans of 9 reflections) effects were applied. The intensities of three standard reflections showed no variations greater than those predicted by counting statistics. The structures were solved by Patterson and Fourier methods and refined by full-matrix least-squares using SHELXS-97.[24] For [**1**]SbF_6 anisotropic displacement parameters were only assigned to the Pt, Sb, Cl and F atoms, the

Table 3 Crystal and refinement data

	[**1**]SbF_6	[**1**]BF_4	[**2**]SbF_6
Formula	$C_{22}H_{17}ClF_6N_3PtSb$	$C_{22}H_{17}BClF_4N_3Pt$	$C_{22}H_{14}ClF_9N_3PtSb$
F_w	789.67	640.73	843.64
Crystal system	orthorhombic	monoclinic	monoclinic
Space group	$Pna2_1$	$P2_1/n$	$P2_1/n$
a/Å	19.64(2)	6.87(2)	6.93(2)
b/Å	18.166(5)	19.489(5)	20.114(5)
c/Å	6.653 (2)	16.500(2)	17.979(2)
β/°	90	101.923(5)	100.750(5)
V/Å^3	2373(3)	2161(8)	2462(8)
Z	4	4	4
D_c/g cm^{-3}	2.210	1.969	2.276
T/K	293(2)	293(2)	293(2)
μ/mm^{-1}	7.20	6.66	6.97
F(000)	1480	1224	1576
Total no. of reflns. measured	2450	3589	4055
Independent reflns.	2146 [R_{int} = 0.0158]	2996 [R_{int} = 0.0219]	3423 [R_{int} = 0.0375]
Reflections observed [$I > 2\sigma(I)$]	1727	2208	2504
Refinement type	F^2	F^2	F^2
R_1[a], wR_2[b] [$I > 2\sigma(I)$]	0.0358, 0.1013	0.0431, 0.1233	0.0449, 0.1160
R_1[a], wR_2[b] [all data]	0.0533, 0.1142	0.0713, 0.1395	0.0745, 0.1317
No. of refined parameters	182	281	335
(shift/esd.)$_{max}$	0.001	0.001	0.000
max, min $\Delta\rho$/e Å^{-3}	0.993, −0.608	0.882, −1.133	2.035, −1.075

[a] $R_1 = \Sigma||F_o| - |F_c||/\Sigma|F_o|$. [b] $wR_2 = [\Sigma[w(F_o^2 - F_c^2)^2]/\Sigma[w(F_o^2)^2]]^{1/2}$ where $w = 1/[\sigma^2(F_o^2) + (0.1P)^2]$ and $P = (F_o^2 + 2F_c^2)/3$.

remaining non-hydrogen atoms being assigned individual isotropic displacement parameters and the hydrogen atoms (in calculated positions) a single overall isotropic displacement parameter. Attempts to carry out a full anisotropic refinement of the non-hydrogen atoms in [**1**]SbF_6 led to problems with atoms N(2) and C(5) being assigned as "non-positive definite". Inverting the absolute structure of [**1**]SbF_6 and re-refining gave a fractionally higher Flack parameter. For [**1**]BF_4 the seven carbon atoms [C(16)–C(22)] of the *o*-tolyl substituent in the 4′-postion of the terpyridyl ring were constrained to lie in the same plane using the SHELXS-97 command "FLAT".[24] This was necessitated because of the high thermal vibration of some of these atoms and the ensuing difficulty experienced in refining them to sensible positions in the absence of the constraint. All the non-hydrogen atoms in [**1**]BF_4 and [**2**]SbF_6 were refined anisotropically while the hydrogen atoms (in calculated positions) were assigned a single overall isotropic displacement parameter. The crystal structure diagrams were produced by the ORTEP program.[25]

CCDC reference numbers 168557–168559.

See http://www.rsc.org/suppdata/dt/b1/b107113k/ for crystallographic data in CIF or other electronic format.

Acknowledgements

We acknowledge financial support from the University of Natal and the South African National Research Foundation. Thanks also go to the United States National Research Foundation for funding through grant CHE 97–26435. We extend our appreciation to Dr Orde Munro for helpful discussions.

References and notes

1 V. H. Houlding and V. M. Miskowski, *Coord. Chem. Rev.*, 1991, **111**, 145.
2 V. M. Miskowski and V. H. Houlding, *Inorg. Chem.*, 1989, **28**, 1529.
3 M. Weiser-Wallfahrer and G. Gliemann, *Z. Naturforsch., Teil B*, 1990, **45**, 652.
4 V. M. Miskowski and V. H. Houlding, *Inorg. Chem.*, 1991, **30**, 4446.
5 V. M. Miskowski, V. H. Houlding, C.-M. Che and Y. Wang, *Inorg. Chem.*, 1993, **32**, 2518.
6 H.-K. Yip, L.-K. Cheng, K.-K. Cheung and C.-M. Che, *J. Chem. Soc., Dalton Trans.*, 1993, 2933.
7 J. A. Bailey, M. G. Hill, R. E. Marsh, V. M. Miskowski, W. P. Schaefer and H. B. Gray, *Inorg. Chem.*, 1995, **34**, 4591.
8 W. B. Connick, L. M. Henling, R. E. Marsh and H. B. Gray, *Inorg. Chem.*, 1996, **35**, 6261.
9 R. Büchner, J. S. Field, R. J. Haines, C. T. Cunningham and D. R. McMillin, *Inorg. Chem.*, 1997, **36**, 3952.
10 R. Büchner, C. T. Cunningham, J. S. Field, R. J. Haines, D. R. McMillin and G. C. Summerton, *J. Chem. Soc., Dalton Trans.*, 1999, 711.
11 F. Kröhnke, *Synthesis*, 1976, 1.
12 K. W. Jennette, J. T. Gill, J. A. Sadownick and S. J. Lippard, *J. Am. Chem. Soc.*, 1976, **98**, 6159; J. A. Bailey, V. M. Miskowski and H. B. Gray, *Acta Crystallogr., Sect. C.*, 1992, **48**, 1420.
13 E. C. Constable, J. Lewis, M. C. Liptrot and P. R. Raithby, *Inorg. Chim. Acta*, 1990, **178**, 47.
14 D. S. Martin, in *Extended Interactions between Metal Ions*, ed. L. V. Interannte, ACS Symp. Ser. 5, American Chemical Society, Washington, DC, 1974, p. 254.
15 C. A. Hunter and J. K. M. Sanders, *J. Am. Chem. Soc.*, 1990, **112**, 5525.
16 W. B. Connick, R. E. Marsh, W. P. Schaefer and H. B. Gray, *Inorg. Chem.*, 1997, **36**, 913.
17 Ref. 18 gives the van der Waals radius of a methyl group as 2.0 Å. The van der Waals radius of 2.3 Å for a trifluoromethyl group was obtained by increasing the van der Waals radius of a methyl group by a distance equal to the difference in the covalent radius for a hydrogen atom and that for a fluorine atom.
18 J. E. Huheey, E. A. Keitner and R. L. Keitner, *Inorganic Chemistry*, HarperCollins, New York, 4th edn., 1993.
19 (*a*) T. K. Aldridge, E. M. Stacey and D. R. McMillin, *Inorg. Chem.*, 1994, **33**, 722; (*b*) D. K. Crites Tears and D. R. McMillin, *Coord. Chem. Rev.*, 2001, **211**, 195; (*c*) the possibility that the structured emission from the dilute glass is due to the presence of free ligand can be discounted because the highest vibronic component in the emission of the free 4′-phenyl-2,2′:6′,2″-terpyridyl ligand is at 435 nm *i.e.*, at a much shorter wavelength than the signal in Fig. 6. See: J. F. Michalec, S. A. Bejune, D. G. Cuttell, G. C. Summerton, J. A. Gertenbach, J. S. Field, R. J. Haines and D. R. McMillin, *Inorg. Chem.*, 2001, **40**, 2193; (*d*) another possibility is that the broad emission shown in Fig. 7 arises from a d–d state. Certainly, Miskowski and co-workers have assigned similar broad emisions as d–d bands in a number of related compounds; see ref. 5.
20 A. I. Kitaigorodskii, *Organic Chemical Crystallography*, Consultants Bureau, New York, 1961.
21 R. E. Peierls, *Quantum Theory of Solids*, Oxford, London, 1953.
22 L. Carlsen, H. Egsgaard and J. R. Anderson, *Anal. Chem.*, 1979, **51**, 1593.
23 F. Liu, K. L. Cunningham, W. Uphues, G. W. Fink, J. Schmolt and D. R. McMillin, *Inorg. Chem.*, 1995, **34**, 2015.
24 G. M. Sheldrick, SHELXS-97, A program for crystal structure determination and refinement, University of Göttingen, 1997.
25 L. Farrugia, *J. Appl. Crystallogr.*, 1997, **30**, 565.